LASER
& PHOTONICS
REVIEWS

Laser Photonics Rev. **9,** No. 6, 713–719 (2015) / **DOI** 10.1002/lpor.201500182

Abstract Conventional optics is diffraction limited due to the cutoff of spatial frequency components, and evanescent waves allow subdiffraction optics at the cost of complex near-field manipulation. Recently, optical superoscillatory phenomena were employed to realize superresolution lenses in the far field, but suffering from very narrow working wavelength band due to the fragility of the superoscillatory light field. Here, an ultrabroadband superoscillatory lens (UBSOL) is proposed and realized by utilizing the metasurface-assisted law of refraction and reflection in arrayed nanorectangular apertures with variant orientations. The ultrabroadband feature mainly arises from the nearly dispersionless phase profile of transmitted light through the UBSOL for opposite circulation polarization with respect to the incident light. It is demonstrated in experiments that subdiffraction light focusing behavior holds well with nearly unchanged focal patterns for wavelengths spanning across visible and near-infrared light. This method is believed to find promising applications in superresolution microscopes or telescopes, high-density optical data storage, etc.

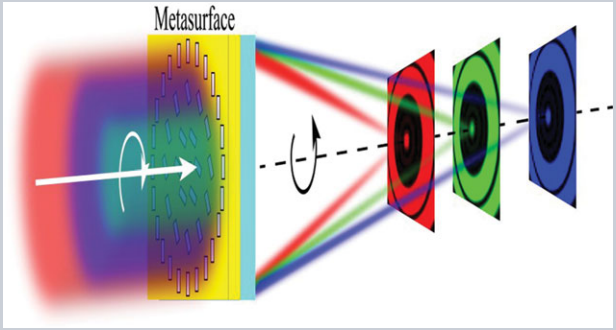

ORIGINAL
PAPER

Ultrabroadband superoscillatory lens composed by plasmonic metasurfaces for subdiffraction light focusing

Dongliang Tang, Changtao Wang, Zeyu Zhao, Yanqin Wang, Mingbo Pu, Xiong Li, Ping Gao, and Xiangang Luo*

1. Introduction

The diffractive nature of light brings a fundamental resolution limit like Abbe–Rayleigh criteria in optical imaging systems. To overcome this obstacle, some superresolution methods in the past decades have been proposed and demonstrated to exploit evanescent waves and surface plasmons delivering high spatial frequency components in imaging process, such as the scanning near-field optical microscopy (SNOM) [1], superlens [2] and hyperlens [3], etc. As the cost of subdiffraction ability, those approaches have been suffering from the complexity of near-field optical manipulations. Recently, optical focusing and imaging beyond the Abbe diffraction limit in the far field were realized by employing a unique optical phenomenon termed as superoscillation [4–15], which occurs in the region where a band-limited light-field function is able to oscillate much faster than its highest frequency component [4, 5]. The optical superoscillatory phenomenon usually arises from the delicate interference of light generated by specially designed structures and is usually featured with a very small fraction of light power and constrained within a small region [6]. The key point to design a superoscillatory element relies on the optimization and generation of complex light fields, including their phase and amplitude distributions, by some special means like spatial light modulators (SLMs) [7,8], optical eigenmodes methods [8,9] and binary masks [10–14]. The superoscillatory phenomenon provides access to subdiffraction optical imaging beyond the near-field constraints. Recently, a subwavelength spot obtained by a superoscillatory lens (SOL) was employed for far-field microscopy imaging with resolution better than $\lambda/6$ [11].

Unfortunately, the SOLs usually exhibit great fragility to the change of light fields due to the delicate light interference behaviors, especially for the spot size far beyond the Abbe diffraction limit [8, 15]. Therefore, the proposed SOLs just realize its subdiffraction focusing within a narrowband of light wavelengths, due to the fact that the light field generated by specially designed structures, like SLMs [7, 8], nanoholes [10] and nanorings [11–14], etc., usually shows a strong dependence on light wavelength.

In this work, an ultrabroadband superoscillatory lens (UBSOL) is realized by employing a metasurface structure composed of arrayed nanoapertures with variant orientations. It is found that the metasurface provides a nearly dispersionless phase profile of transmitted light for opposite circulation polarization with respect to the incident light. The slight variation of the light field under the paraxial approximation promises that the subdiffraction focusing behavior holds well for a wide range of light wavelengths. As demonstrated in experiments, superoscillatory focal patterns with the full-width-at-half-maximum (FWHM) being about 0.674 times the spot size of the Abbe diffraction limit are observed in the visible and near-infrared light wavelength range. It is believed that this method could find promising applications such as white-light

State Key Lab of Optical Technologies on Nano-fabrication and Micro-engineering, Institute of Optics and Electronics, Chinese Academy of Sciences, P.O. Box 350, Chengdu, 610209, China
*Corresponding Author: E-mail: lxg@ioe.ac.cn

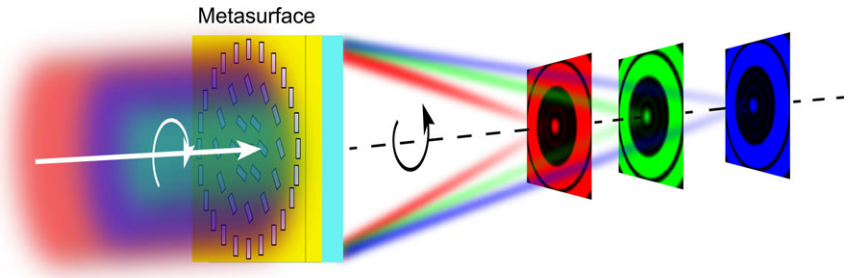

Figure 1 Schematic of ultrabroadband subdiffraction focusing with superoscillatory plasmonic metasurface.

superresolution microscopes, high-density optical storage with multiple wavelengths, etc.

2. Principle and design

As illustrated in Fig. 1, the proposed UBSOL is realized by a specially designed metasurface structure inscribed on a metal film, which consists of a great number of transparent rectangular nanoapertures with variant orientations. A plane wave with left or right circular polarization is normally incident on the UBSOL. The transmitted light for crosspolarization with respect to the incidence possesses a specific geometric phase profile [16–18], which shows a nearly dispersionless feature [17] and allows the nearly same subdiffraction light focusing patterns at variant focal planes for broadband light wavelengths. This focusing behavior could be well understood by utilizing the metasurface-assisted law of refraction and reflection [19]

$$\begin{cases} n_1 k_0 \sin\theta_1 + \nabla\Phi = n_1 k_0 \sin\theta_3 \\ n_1 k_0 \sin\theta_1 + \nabla\Phi = n_2 k_0 \sin\theta_2, \end{cases} \quad (1)$$

where $\nabla\Phi$ is the designed phase gradient at the metasurface plane and is determined by the geometric structures, n_1 and n_2 are the refractive indices of the media at the incident and transmitted sides, θ_1, θ_2 and θ_3 are the angles for incident, refracted, and reflected light.

The unique dispersionless phase manipulation of a metasurface structure for light with circular polarization plays the key role in designing an UBSOL. To show this point, light response and dispersion analysis are presented in Fig. 2. As a representative structure, the metasurface is assumed to be periodically arrayed rectangular nanometallic apertures with fixed orientation, 200 × 200 nm period, 140 nm length, 60 nm width and 120 nm thickness, as shown in Fig. 2a. Full-wave simulations are performed by CST Microwave Studio to calculate the response of nanoapertures for circular polarization incidence.

As light with circular polarization impinges at the nanorectangular metallic aperture, localized plasmonic modes within the aperture would be excited and help to squeezing light through the nanoaperture with subwavelength dimensions. As a reasonable approximation, each nanoaperture could be considered as a plasmonic dipole antenna [17], through which the transmitted light field is partially converted to its opposite helicity with an abrupt phase

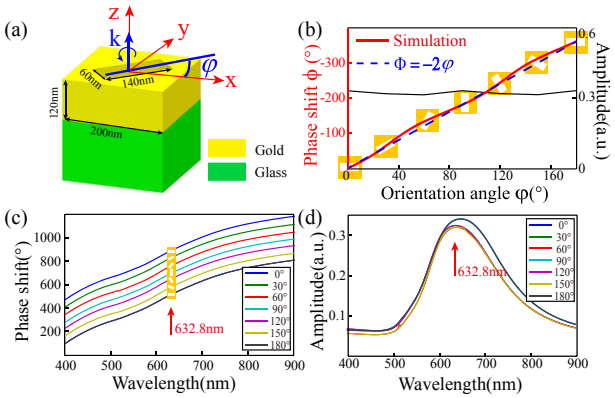

Figure 2 (a) Schematic of the unit-cell nanoaperture. (b) Phase shift and amplitude as a function of orientation angle at the wavelength of 632.8 nm. (c) Phase shift and (d) amplitude of light through nanoaperture with variant orientation for incident wavelength from 400 nm to 900 nm.

change Φ, governed by $\Phi = \pm 2\varphi$, with φ being the orientation angle ranging from 0° to 180°, the + sign standing for right circular polarization (RCP) incidence converted to left circular polarization (LCP) transmission and the – sign for LCP converted to RCP. This phase modulation is demonstrated in Fig. 2b for LCP incidence at the wavelength of 632.8 nm, where the phase shift changes from 0° to −360° with a linear relation with aperture orientation angles. The slight deviation is mainly attributed to the angle dependence of light interaction between neighboring apertures. As the phase shift is independent of the light wavelength, the phase change values are approximately fixed under a broad spectrum from 400 nm to 900 nm, as shown in Fig. 2c, which ensures a nearly dispersionless phase profile generated by a metasurface. The bandwidth can be further increased by using the continuous catenary structure, which eliminates the resonance of nanoresonators and guarantees the conversion efficiency in an ultrabroadband frequency range [20].

On the other hand, the amplitude of the transmitted light through the nanoaperture with opposite circular polarization shows some plasmonic resonance with light wavelengths, as shown in Fig. 2d where the resonant wavelength is around 632.8 nm and the amplitude decreases obviously for wavelengths ranging from 400 nm to 900 nm. The good aspect is that the transmission ampli-

tudes change slightly for variant aperture orientation angles from 0° to 180°. The calculated maximum amplitude deviation is about 0.018 for 632.8 nm wavelength. Thus, it is reasonable to assume in our designs and calculations that the amplitudes are uniform for transmitted light through the nanoapertures with variant orientations at a single wavelength.

The design of an UBSOL is first to determine the phase profile required for subdiffraction focusing at a single wavelength. To do this, the phase is viewed as a combination of a hyperboloidal phase profile $\Phi_{\text{lens}}(r)$ for light focusing and an extra phase modulation $\Phi_{\text{binary}}(r)$ for superoscillatory behavior beyond the Abbe diffraction limit. The first part could be written as [21]

$$\Phi_{\text{lens}}(r) = \frac{2\pi}{\lambda_0}\left(-\sqrt{{f_0}^2 + r^2} + f_0\right) + 2m\pi, \qquad (2)$$

where λ_0 is the central light wavelength, f_0 is the focal length, m is an integer.

As for the extra phase part $\Phi_{\text{binary}}(r)$, it is assumed to be a circular symmetrical binary phase function (0 or π) with finite phase-jump positions. In this work, the positions are optimized by linear programming method [22, 23] to obtain a subdiffraction focal spot for the converted circular polarized light, defined by the Fresnel diffraction integral equation around the focal plane [24],

$$I(\lambda, \rho, z) \propto \left(\frac{1}{\lambda z}\right)^2 \left| \int_0^R \exp\left[i\Phi_{\text{binary}}(r) + i\Phi_{\text{lens}}(r)\right] \times \exp\left(i\pi r^2 \frac{1}{\lambda z}\right) J_0\left(\frac{2\pi r\rho}{\lambda z}\right) \text{rdr} \right|^2. \qquad (3)$$

In the paraxial region, the hyperboloidal phase profile of Eq. (2) could be further approximately expressed as

$$\Phi_{\text{lens}}(r) \approx -\frac{\pi r^2}{\lambda_0 f_0} + 2m\pi. \qquad (4)$$

Using Eq. (4), Eq. (3) is rewritten as

$$I(\lambda, \rho, z) \propto \left(\frac{1}{\lambda z}\right)^2 \left| \int_0^R \exp\left[i\Phi_{\text{binary}}(r)\right] \times \exp\left[i\pi r^2\left(\frac{1}{\lambda z} - \frac{1}{\lambda_0 f_0}\right)\right] J_0\left(\frac{2\pi r\rho}{\lambda z}\right) \text{rdr} \right|^2. \qquad (5)$$

In our previous work, we have shown that a properly designed phase profile can obtain superresolution imaging in a telescope system [19a]. In the following, three designed examples are presented with $\Phi_{\text{binary}}(r)$ plotted in Fig. 3a. As a control case of modulation phase $\Phi_{\text{binary}}(r) = 0$ (for Sample A), the design turns to be a conventional focusing lens with an Airy spot at the focal plane. The other two designs of $\Phi_{\text{binary}}(r)$ account for UBSOLs with different FWHMs beyond the Abbe diffraction limit. Their simulated focal

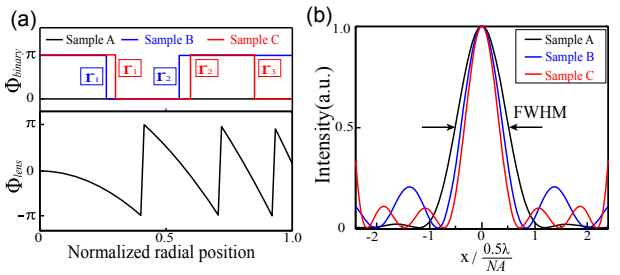

Figure 3 (a) Designed phase profiles for UBSOLs with Samples A, B and C. Bottom: hyperboloidal phase profile localized in $[-\pi, \pi]$. Top: optimized extra phase jump functions. Sample A: without π-phase-jump; Sample B: π-phase-jump at positions $r_1 = 0.262$ and $r_2 = 0.556$; Sample C: at positions $r_1 = 0.297$, $r_2 = 0.594$ and $r_3 = 0.85$. (b) Theoretical light distributions at the focal plane for Samples A, B and C.

patterns are plotted in Fig. 3b. The first one (for Sample B) is to generate a 0.807 times the spot size of the Abbe diffraction limit hotspot without significant side lobes, less than 20% of the peak intensity. Also, a smaller focusing spot with spot size being 0.678 of the Abbe diffraction limit (for Sample C) is achieved with a limited field of view and much higher side lobes around it. The field of view in Sample C, defined as the area of low intensity less than 10% of the central intensity, could be used for real-time superresolution imaging [7]. In theory, it is possible to get an arbitrarily small focal spot beyond the Abbe diffraction limit at the focal plane. But this usually delivers very small focal intensity and is utterly fragile to phase-profile aberrations, calculation precision and fabrication errors [6, 8]. As seen in Fig. 2c, the slight phase variation with maximum deviation of about 12.5° for variant light wavelengths may greatly degrade the subdiffraction focal spot of UBSOL in this case.

Although the metasurface structure delivers a nearly dispersionless phase distribution of transmitted light with opposite circular polarization for variant light wavelengths, large focus shift would occur owning to the axial chromatic aberration of phase profile defined in Eq. (2). Under the paraxial approximation, the chromatic focus shift follows the rule that the product λz is kept to be nearly a constant [17]. It should be noted here that, for those wavelengths away from the designed central wavelength, the modulated phase function of transmitted light defined by Eq. (2) is not a perfect hyperboloidal phase distribution for the shifted focus position. Fortunately, these phase aberrations are usually small under paraxial approximation and would allow nearly unchanged superoscillatory focal patterns around the shifted focal plane for a wide range of light wavelengths, which could be well understood by substituting $\lambda z \approx \lambda_0 f_0$ into Eq. (5) and we have

$$I(\rho) \propto \left(\frac{1}{\lambda_0 f_0}\right)^2 \left| \int_0^R \exp\left[i\Phi_{\text{binary}}(r)\right] J_0\left(\frac{2\pi r\rho}{\lambda_0 f_0}\right) r dr \right|^2. \qquad (6)$$

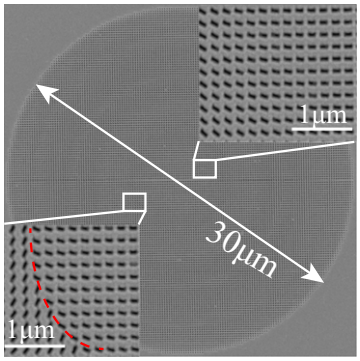

Figure 4 Scanning electron microscopy image of Sample C. The inset shows the section with varying orientations and the red-dashed line indicates phase-jump positions.

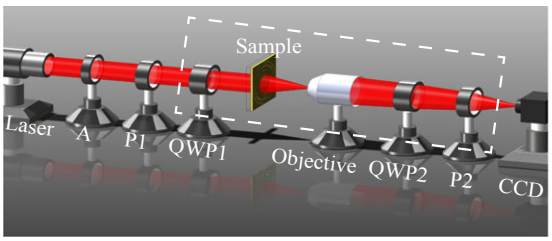

Figure 5 Schematic of setup for the measurement of UBSOL focusing patterns. A: attenuator. P: linear polarizer. QWP: quarter-wave plate. The elements in the dashed line are mounted in a customized microscope.

3. Experimental section

Three metasurface structures, with outer diameter $D = 30$ μm having a focal length $f_0 = 60$ μm at the wavelength $\lambda_0 = 632.8$ nm for LCP incidence, are designed based on the phase modulation feature of nanoapertures in Fig. 2 and the desired phase functions in Fig. 3. The structures are manufactured by focused-ion-beam (FIB) milling on a 120-nm thick gold film deposited on a glass substrate. Figure 4 shows the scanning electron microscopy image for Sample C. The right-top inset with magnification shows the central section with varying orientations and the red-dashed line in the left-bottom inset indicates phase-jump positions nearly corresponding to the nanoapertures' orientation angle shift of 90°. As the metasurfaces are illuminated with LCP light at the wavelength of 632.8 nm, the desired subdiffraction focusing spots for the transmitted RCP light are observed and measured with the schematic optical measurement setup shown in Fig. 5, including an attenuator, two quarter-wave plates (QWPs), two linear polarizers, an objective and a CCD camera. The elements in the dashed line are mounted in a customized microscope. A circularly polarized laser beam is generated by a QWP and a polarizer in front of the sample. The transmitted light through the sample is collected by a 100×/0.85 objective and filtered for the

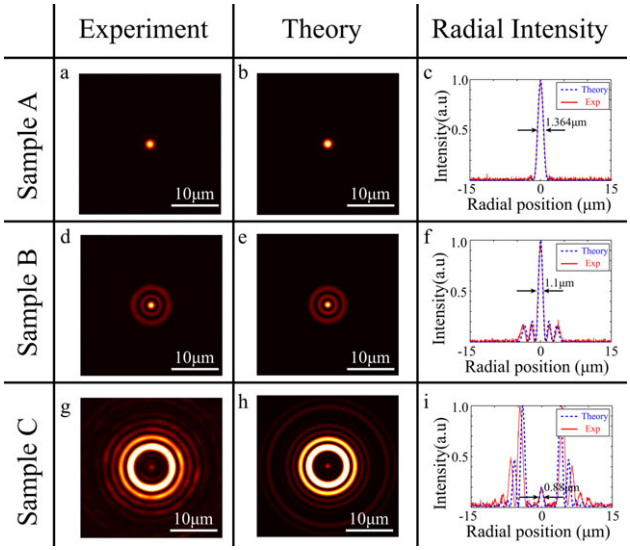

Figure 6 (a, b, d, e, g, h) Experimental and theoretical light distributions at the focal plane for Samples A, B and C with fixed wavelength of 632.8 nm, respectively. (c, f, i) Normalized light distributions along the radial direction for the three samples, respectively.

light with opposite circular polarization by another pair of QWP and polarizer. The imaged patterns are recorded with a CCD camera (WinCamD-UCD15, 1200×1200, pixel size 4.4 μm) and scanned in the z direction with step of 1 μm.

4. Results and discussions

In Fig. 6, the measured light distributions at the focal plane of $z = 60$ μm are presented and show good agreement with theoretical calculations. The measured focusing FWHM for Sample A is 1.364 μm, very close to the calculated Abbe diffraction limit of $0.5\lambda/\mathrm{NA} = 1.304$ μm, with calculated numerical aperture NA = 0.2425. The focal FWHMs for Sample B and Sample C are measured to be 1.1 μm and 0.88 μm, about 0.843 and 0.674 times the spot size of the Abbe diffraction limit, respectively. The slight discrepancy of the side lobes between the experimental and theoretical results for the Sample C may be attributed to the enhanced fragility to fabrication errors for deep subdiffraction focusing.

Figure 7 shows the measured light distributions for the three samples with light wavelengths of 405 nm, 532 nm, 632.8 nm and 785 nm, respectively. Clearly, the focal patterns show almost similar optical-field distributions, except for the large chromatic focus shift from 93 μm to 48 μm and the change of focusing intensity. The light distributions at variant focal planes show nearly the same profiles as shown in the bottom panel of Fig. 7. This invariance of diffraction patterns, as discussed above, benefits from the chromatic focus shift defined by the constant λz under the paraxial approximation, which enables the focal patterns defined by Eq. (6) to show invariance with respect to light wavelengths. In other words, the change of focal

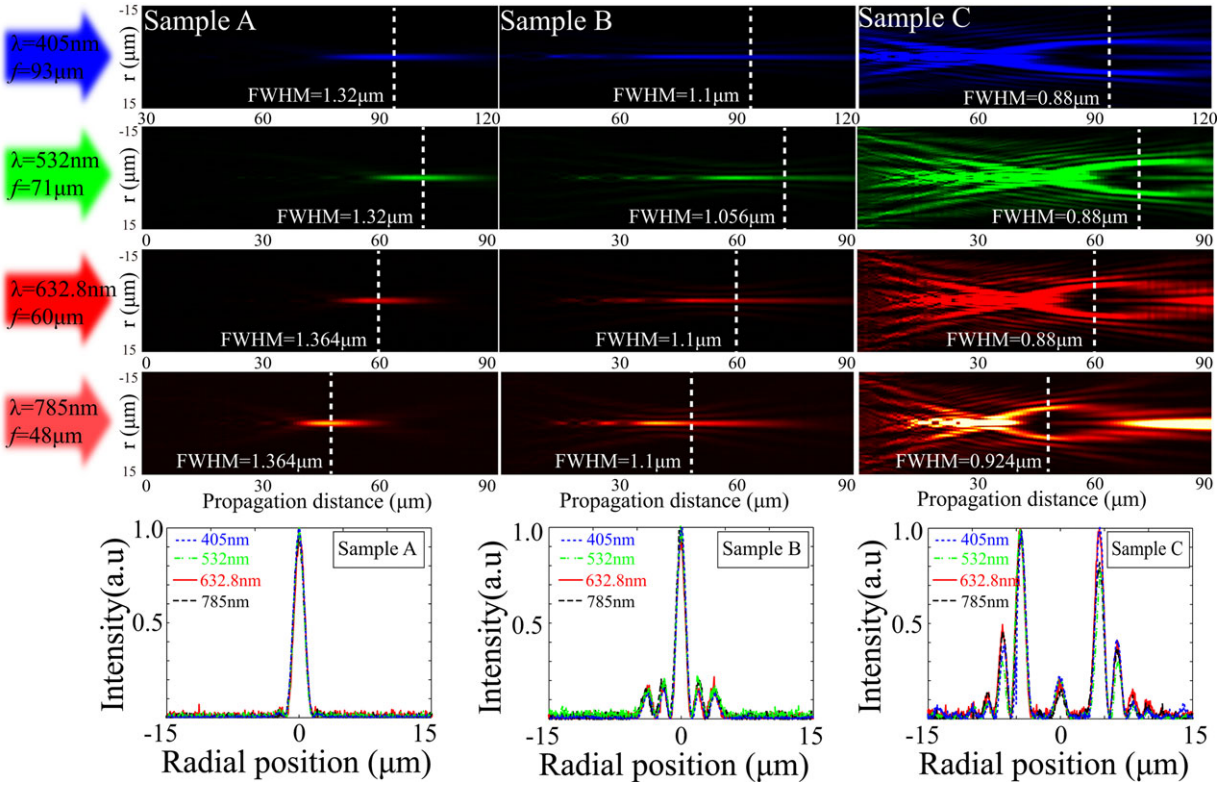

Figure 7 Top: experimental light distributions along the *z* direction for Sample A, B and C at wavelengths of 405 nm, 532 nm, 632.8 nm and 785 nm, respectively. Bottom: normalized intensity distributions at the focal plane for the three samples with variant wavelengths. Note that the first row for 405-nm light wavelength plots with distance from 30 μm to 120 μm, and the other rows from 0 μm to 90 μm.

patterns for variant light wavelengths is compensated by the axial chromatic focus shift. The invariant feature of light distributions for variant wavelengths still holds for a wide *z*-axis positions region, where the approximation of Eq. (5) keeps its validity. In addition, Sample B shows a needle-like behavior [14, 25] with greatly elongated depth of focus in contrast to the Airy spot in Sample A. The needle-like focusing behavior is related to the diffraction pattern invariance feature of nondiffracting Bessel beams and in the design of Sample B the modulation of phase profile happens to generate the similar effect, which could also be seen in some references using diffractive optical elements under radially or circularly polarized light [25]. For the Sample C, the focal pattern, exhibiting greatly reduced spot size in the central dark region, is featured with a much shallower depth of focus due to its fragility of superoscillatory spot.

The low efficiency is a common concern for both transmitted-type metasurfaces and superoscillatory focus. The transmission efficiency, focusing efficiency and central focus peak intensity for the three samples are shown in Table 1. It is worth noting that most of the light energy of SOL is contributed to the large side lobes around the central subdiffraction hotspot, especially for those SOL spots with very small lateral size, and the cost of energy is inevitable in superoscillatory phenomenon but there is a tradeoff between subdiffraction spot size and focusing efficiency [6]. On the other hand, the metasurface usually shows very low transmission, as demonstrated in our paper that the transmission of nanoaperture is about 10% at the central wavelength of 632.8 nm and much lower for wavelengths away from it. So, it is not surprising that the focusing efficiencies for Samples A, B and C are only 8.38%, 1.29% and 0.024%, respectively. This cost of low efficiency would be acceptable, considering that some subdiffraction methods like SNOM characterized with ultralow transmission efficiency through nanofiber apertures and complex near-field manipulation [1, 2]. Fortunately, what we are concerned with is the SOL's subdiffraction focusing behavior in the far field, which could hold over a wide range of light wavelengths benefiting from the unique phase-modulation feature of metasurface, and the low focusing efficiency of SOL could be applicable in practical applications with high-power laser sources and high-sensitivity detectors. In principle, the conversion efficiency could be increased by using a reflective layer to suppress the undesired scattering [26]. In the meantime, the operating bandwidth could be maximized by engineering the dispersion of the metasurfaces [26, 27], according to the revised Fresnel's equations in multilayered metasurfaces [19a].

It is hard to give a definite wavelength range for the proposed UBSOL. As for light with much shorter wavelength and enlarged focal length, the finite size of nanoapertures would bring greater phase aberration due to light interactions between neighboring apertures and the aberration

Table 1 Light-transmission efficiency, peak intensity and efficiency of central spot for Samples A, B and C with variant wavelengths. The incident light intensity is assumed to be 1.

Wavelength	405 nm			532 nm			632.8 nm			785 nm		
Sample	A	B	C	A	B	C	A	B	C	A	B	C
Relative size to diffraction limit	1.03	0.807	0.662	1.03	0.807	0.696	1.03	0.807	0.678	1.03	0.809	0.69
Light transmission efficiency (%)	0.35	0.35	0.35	0.95	0.95	0.95	10	10	10	1.95	1.95	1.95
Peak intensity of central spot	2.4	0.64	0.016	6.36	1.67	0.043	65.3	16.9	0.4	12.5	3.2	0.078
Efficiency of central spot (%)	0.29	0.046	0.0009	0.8	0.12	0.002	8.38	1.29	0.024	1.63	0.25	0.005

may contribute negatively to the superoscillatory focusing. In theory, the subdiffraction focusing performances of Sample B and C may be observed for much longer wavelengths in the near-infrared region. However, this would deliver a shorter focal length and a greater focal pattern variance, as the approximation of Eq. (5) would not hold perfectly. On the other hand, the longitudinal electrical component would be increased obviously and deliver wider lateral focus size in the case of high numerical aperture and circular or linear light polarization [28]. So the subdiffraction focusing feature would be greatly diminished for focus size evaluation with total electrical field intensity as demonstrated in some references [14a, 25b]. In some investigations, radially polarized light incidence and vectorial angular spectrum theory were employed to generate SOLs with high numerical apertures, where the longitudinal components dominated the focus intensity distribution and the transverse components contributed negatively to the focus size [12a, 12b, 25a]. A recent study demonstrated that light incidence with azimuthally polarized light and vortical phase helped to generate subdiffraction focus mainly determined by transverse component, and the longitudinal component with very small magnitude showed nearly no contribution to the focus size [14b].

5. Conclusion and outlook

In summary, an ultrabroadband superoscillatory lens (UBSOL) is proposed and demonstrated in this work. It is found that the unique dispersionless feature of phase modulation of light through nanoapertures with variant orientations helps to generate a nearly unchanged phase profile over a wide light wavelength range. On the other hand, the axial focus shift due to chromatic aberration helps to deliver a nearly fixed subdiffraction focal pattern under the paraxial approximation. As demonstrative examples, subdiffraction focal patterns through UBSOLs for ultrabroadband wavelengths spanning visible and near-infrared light were realized and observed in experiments. From the viewpoint of Fourier optics, the subdiffraction pattern at the focal plane based on the superoscillatory phenomenon could be attributed to the destructive interference of high and low Fourier components, which help to deliver some accessible information beyond the cut-off frequency caused by the finite aperture size of the lens. This feature, we believe, would be the fundamental factor for realizing superresolution imaging optics, especially for some telescope systems, which could not refer to present near-field or fluorescent superresolution methods like a perfect lens with negative refractive index and stimulated emission depletion microscopes. Also, the broadband behavior is helpful to provide a promising access to broadband far-field optics beyond the Abbe diffraction limit, such as white-light superresolution microscopes, spectroscopes and colorful holograms, etc.

Acknowledgements. The authors Dongliang Tang, Changtao Wang, Zeyu Zhao contributed equally to this work. This work was supported by 973 Program of China (No. 2013CBA01700), Chinese Nature Science Grant (61138002, 61177013).

Received: 3 August 2015, **Revised:** 27 August 2015, **Accepted:** 7 September 2015

Published online: 29 September 2015

Key words: ultrabroadband, superoscillatory lens, plasmonic metasurfaces, subdiffraction.

References

[1] E. Betzig, J. K. Trautman, T. D. Harris, J. S. Weiner, and R. L. Kostelak, Science **251**, 1468–1470 (1991).
[2] (a) J. B. Pendry, Phys. Rev. Lett. **85**, 3966–3969 (2000); (b) X. Luo, and T. Ishihara, Appl. Phys. Lett. **84**, 4780–4782 (2004); (c) N. Fang, H. Lee, C. Sun, and X. Zhang, Science **308**, 534–537 (2005).
[3] (a) Z. Liu, H. Lee, Y. Xiong, C. Sun, and X. Zhang, Science **315**, 1686 (2007); (b) X. Luo, and L. Yan, IEEE Photonics J. **4**, 590 (2012).
[4] (a) M. V. Berry, and S. Popescu, J. Phys. A: Math. Gen. **39**, 6965–6977 (2006); (b) E. Greenfield, R. Schley, I. Hurwitz, J. Nemirovsky, K. G. Makris, and M. Segev, Opt. Express **21**, 13425 (2013).
[5] P. J. S. G. Ferreira and A. Kempf, IEEE Trans. Signal Process **54**, 3732–3740 (2006).
[6] E. T. F. Rogers and N. I. Zheludev, J. Opt. **15**, 094008 (2013).
[7] A. M. H. Wong and G. V. Eleftheriades, Sci. Rep. **3**, 1715 (2013).

[8] S. Kosmeier, M. Mazilu, J. Baumgartl, and K. Dholakia, J. Opt. **13**, 105707 (2011).
[9] J. Baumgartl, S. Kosmeier, M. Mazilu, E.T. F. Rogers, N. I. Zheludev, and K. Dholakia, Appl. Phys. Lett. **98**, 181109 (2011).
[10] F. M. Huang, T. S. Kao, V. A. Fedotov, Y. Chen, and N. I. Zheludev, Nano Lett. **8**, 2469–2472 (2008).
[11] E. T. F. Rogers, J. Lindberg, T. Roy, S. Sove, J. E. Chad, M. R. Dennis, and N. I. Zheludev, Nature Mater. **11**, 432–435 (2012).
[12] (a) H. Ye, C.-W. Qiu, K. Huang, J. Teng, B. Luk'yanchuk, and S. P. Yeo, Laser Phys. Lett. **10**, 065004 (2013); (b) T. Liu, J. Tan, J. Liu, and H. Wang, Opt. Express **21**, 15090–15101 (2013).
[13] K. Huang, H. Ye, J. Teng, S.P. Yeo, B. Luk'yanchuk, and C.-W. Qiu, Laser Photon. Rev. **8**, 152–157 (2014).
[14] (a) G. Yuan, E. T. F. Rogers, T. Roy, G. Adamo, Z. Shen, and N. I. Zheludev, Sci. Rep. **4**, 6333 (2014); (b) F. Qin, K. Huang, J. Wu, J. Jiao, X. Luo, C.-W. Qiu, and M. Hong, Sci. Rep. **5**, 09977 (2015).
[15] H. J. Hyvärinen, S. Rehman, J. Tervo, J. Turunen, and C. J. R. Sheppard, Opt. Lett. **37**, 903–905 (2012).
[16] E. Hasman, V. Kleiner, G. Biener, and A. Niv, Appl. Phys. Lett. **82**, 328–330 (2003).
[17] L. Huang, X. Chen, H. Mühlenbernd, H. Zhang, S. Chen, B. Bai, Q. Tan, G. Jin, K.-W. Cheah, C.-W. Qiu, J. Li, T. Zentgraf, and S. Zhang, Nature Commun. **4**, 2808 (2013).
[18] D. Lin, P. Fan, E. Hasman, and M. L. Brongersma, Science **345**, 298–302 (2014).
[19] (a) X. Luo, Science China-Phys., Mech. Astron. **58**, 594201 (2015); (b) X. Luo, M. Pu, X. Ma, and X. Li, Int. J. Antenn. Propag. **2015**, 204127 (2015).
[20] M. Pu, X. Li, X. Ma, Y. Wang, Z. Zhao, C. Wang, C. Hu, P. Gao, C. Huang, H. Ren, X. Li, F. Qin, J. Yang, M. Gu, M. Hong, and X. Luo, Sci. Adv. **1**, e1500396 (2015).
[21] E. Hecht, Optics, 3rd edn (Addison Wesley Publishing Company: Reading, MA, 1997).
[22] G. Toraldo di Francia, Suppl. Nuovo Cim. **9**, 426–438 (1952).
[23] H. Liu, Y. Yan, Q. Tan, and G. Jin, J. Opt. Soc. Am. **19**, 2185–2193 (2002).
[24] M. Born and E. Wolf, Principles of Optics: Electromagnetic Theory of Propagation, Interference and Diffraction of Light, 6th ed. (Cambridge University Press, UK, 1999).
[25] (a) H. Wang, L. Shi, B. Luk'yanchuk, C. Sheppard, and C. T. Chong, Nature Photon. **2**, 501–505 (2008); (b) J. S. Wei, Y. K. Zha, and F. X. Gan, Prog. Electromagn. Res. **140**, 589–598 (2013).
[26] (a) G. Zheng, H. Mühlenbernd, M. Kenney, G. Li, and S. Zhang, Nat. Nanotechnol. **10**, 308 (2015); (b) M. Pu, Z. Zhao, Y. Wang, X. Li, X. Ma, C. Hu, C. Wang, C. Huang, and X. Luo, Sci. Rep. **5**, 9822 (2015).
[27] (a) M. Pu, P. Chen, Y. Wang, Z. Zhao, C. Huang, C. Wang, X. Ma, and X. Luo, Appl. Phys. Lett. **102**, 131906 (2013); (b) Q. Feng, M. Pu, C. Hu, and X. Luo, Opt. Lett. **37**, 2133–2135 (2012).
[28] (a) Q. W. Zhan, Opt. Lett. **31**, 867–869 (2006); (b) G. M. Lerman, and U. Levy, Opt. Exp. **16**, 4567–4581 (2008).